



# Prediction of Isocitrate Dehydrogenase Genotype in Brain Gliomas with MRI: Single-Shell versus Multishell Diffusion Models

Matteo Figini, PhD • Marco Riva, MD • Mark Graham, MSc • Gian Marco Castelli, MSc • Bethania Fernandes, MD • Marco Grimaldi, MD • Giuseppe Baselli, MSc • Federico Pessina, MD • Lorenzo Bello, MD • Hui Zhang, PhD • Alberto Bizzi, MD

From the Departments of Scientific Direction (M.F.) and Neuroradiology (G.M.C., A.B.), Fondazione IRCCS Istituto Neurologico Carlo Besta, via Celoria 11, 20133 Milan, Italy; Department of Medical Biotechnology and Translational Medicine (M.R.) and Department of Oncology and Hemato-Oncology (L.B.), Università degli Studi di Milano, Milan, Italy; Unit of Surgical Neuro-Oncology (M.R., F.P., L.B.), Department of Pathology (B.F.), and Department of Radiology (M. Grimaldi), Humanitas Research Hospital, Milan, Italy; Centre for Medical Image Computing & Department of Computer Science, University College London, London, England (M. Graham, H.Z.); and Department of Electronics, Information and Bioengineering, Politecnico di Milano, Milan, Italy (G.B.). Received January 7, 2018; revision requested February 28; final revision received July 23; accepted August 8. **Address correspondence to** A.B. (e-mail: [alberto\\_bizzi@fastwebnet.it](mailto:alberto_bizzi@fastwebnet.it)).

Supported by FP7 Information and Communication Technologies (CONNECT-Consortium of Neuroimagers for the Noninvasive Assessment of Brain Connectivity and Tracts). M.R. was supported by Fondazione Italiana per la Ricerca sul Cancro (Fellowship for Abroad 2013). M.G. was supported by the Engineering and Physical Sciences Research Council (EP/L504889/1) and the Engineering and Physical Sciences Research Council Centre for Doctoral Training (EP/L016478/1). H.Z. was supported by the Engineering and Physical Sciences Research Council (EP/N018702/1) and the Medical Research Council (MR/L011530/1). M.G. and H.Z. were additionally sponsored by the Royal Society International Exchange Scheme with China.

Conflicts of interest are listed at the end of this article.

Radiology 2018; 00:1–9 • <https://doi.org/10.1148/radiol.2018180054> • Content codes:  

**Purpose:** The primary aim of this prospective observational study was to assess whether diffusion MRI metrics correlate with isocitrate dehydrogenase (IDH) status in grade II and III gliomas. A secondary aim was to investigate whether multishell acquisitions with advanced models such as neurite orientation dispersion and density imaging (NODDI) and diffusion kurtosis imaging offer greater diagnostic accuracy than diffusion-tensor imaging (DTI).

**Materials and Methods:** Diffusion MRI ( $b = 700$  and  $2000 \text{ sec/mm}^2$ ) was performed preoperatively in 192 consecutive participants (113 male and 79 female participants; mean age, 46.18 years; age range, 14–77 years) with grade II ( $n = 62$ ), grade III ( $n = 58$ ), or grade IV ( $n = 72$ ) gliomas. DTI, diffusion kurtosis imaging, and NODDI metrics were measured in regions with or without hyperintensity on diffusion MR images and compared among groups defined according to IDH genotype, 1p/19q codeletion status, and tumor grade by using Mann-Whitney tests.

**Results:** In grade II and III IDH wild-type gliomas, the maximum fractional anisotropy, kurtosis anisotropy, and restriction fraction were significantly higher and the minimum mean diffusivity was significantly lower than in IDH-mutant gliomas ( $P = .011$ ,  $P = .002$ ,  $P = .044$ , and  $P = .027$ , respectively); areas under the receiver operating characteristic curve ranged from 0.72 to 0.76. In IDH wild-type gliomas, no difference among grades II, III, and IV was found. In IDH-mutant gliomas, no difference between those with and those without 1p/19q loss was found.

**Conclusion:** Diffusion MRI metrics showed correlation with isocitrate dehydrogenase status in grade II and III gliomas. Advanced diffusion MRI models did not add diagnostic accuracy, supporting the inclusion of a single-shell diffusion-tensor imaging acquisition in brain tumor imaging protocols.

Published under a CC BY 4.0 license.

Online supplemental material is available for this article.

A recent update of the World Health Organization (WHO) classification of brain tumors introduced molecular markers that add greater prognostic accuracy than histopathologic findings alone (1,2). Isocitrate dehydrogenase (IDH) genotype and epigenetic 1p/19q codeletion are two key molecular markers. Patients with IDH wild-type gliomas have a worse prognosis than those with IDH-mutant gliomas. Patients with 1p/19q uncodeleted gliomas have a worse prognosis than those with codeleted IDH-mutant gliomas (3). The establishment of in vivo biomarkers that enable prediction of IDH and 1p/19q status would thus be relevant for patient management (4) and clinical trials.

Diffusion MRI is a potential method for providing such in vivo biomarkers. It enables assessment of the

microstructure of the whole tumor at a relatively high spatial resolution and is easily accessible. Diffusion-tensor imaging (DTI) is currently the most used method (5). DTI parameters such as mean diffusivity (MD) and fractional anisotropy (FA) correlate with changes in cellular density and in extracellular matrix features induced by glioma infiltration and growth.

Several studies aimed to grade gliomas with use of DTI. Most of these have demonstrated significantly lower MD values in high-grade gliomas (6–12), but the majority failed to differentiate WHO grade II gliomas from grade III gliomas due to overlapping MD and FA values. A limitation of the above studies is that the authors did not stratify patients according to IDH

## Abbreviations

DTI = diffusion-tensor imaging, FA = fractional anisotropy, IDH = isocitrate dehydrogenase, KA = kurtosis anisotropy, MD = mean diffusivity, NODDI = neurite orientation dispersion and density imaging, ROI = region of interest, WHO = World Health Organization

## Summary

Diffusion metrics from three models correlated with isocitrate dehydrogenase genotype in grade II and III gliomas. Advanced diffusion models did not add significant diagnostic accuracy. Diffusion-tensor imaging plays a role in the identification of those who may benefit from more aggressive treatments despite lacking high-grade features at neuropathologic examination.

## Implications for Patient Care

- Metrics derived from diffusion-tensor imaging, diffusion kurtosis imaging, and neurite orientation dispersion and density imaging correlated with isocitrate dehydrogenase genotype in grade II and III (ie, lower-grade) gliomas.
- The results of diffusion-tensor imaging and multishell advanced models were comparable in the identification of those patients who may require more aggressive treatment due to worse prognosis despite being classified as having a lower-grade glioma with neuropathologic examination.
- Diffusion MRI has the potential to contribute to stratifying patients with lower-grade glioma in clinical trials.

genotype. Only the authors of recent retrospective DTI studies have stratified lower-grade gliomas by IDH and 1p/19q status. They have reported lower apparent diffusion coefficient and higher FA values in IDH wild-type astrocytomas (13) and oligodendrogliomas (14) but no significant differences between gliomas with and gliomas without 1p/19q loss (15). If confirmed in a large prospective study, these findings would expand the use of DTI in gliomas.

Other investigators have shown that advanced models with a high  $b$  value provide better performance than DTI with regard to glioma grading. Diffusion kurtosis imaging (16) parameters, most commonly mean kurtosis and kurtosis anisotropy (KA), can help characterize the non-Gaussian diffusion contribution. Higher mean kurtosis values have been reported in high-grade compared with low-grade gliomas (17,18). Alternatively, multicompartiment models have been proposed to improve specificity to brain microstructure by measuring the diffusion of water molecules in different compartments. One such model is neurite orientation dispersion and density imaging (NODDI) (19). NODDI separates the contribution of three main tissue compartments where water diffusion is restricted, hindered, or free. NODDI parameters such as restriction fraction, isotropic fraction, and orientation dispersion index might be more sensitive to glioma microstructure than are conventional DTI metrics. A multishell acquisition protocol is required for application of advanced diffusion models, with the drawback that it increases imaging time. Therefore, it would be important to assess whether advanced models with high  $b$  values would also be beneficial in stratifying lower-grade gliomas according to IDH status.

Our study of a large population of patients with gliomas was conceived with a prospective design to confirm whether

diffusion MRI metrics correlate with IDH genotype. We tested the hypothesis that IDH wild-type lower-grade gliomas have foci of significantly lower diffusivity and higher restricted fraction. In addition, we investigated whether advanced models such as NODDI and diffusion kurtosis imaging would offer greater diagnostic accuracy than DTI.

## Materials and Methods

### Participants

All participants gave informed written consent for the surgical procedure and this prospective study, according to the World Medical Association Declaration of Helsinki statement for research involving human subjects. This prospective study was approved by the local institutional review board and performed between April 2012 and November 2015. Patients were included in this study if (a) MRI with multishell diffusion was performed less than 2 weeks before surgery and (b) glioma was diagnosed with histopathologic examination and molecular analysis. Patients who had previously undergone brain surgery were included. Exclusion criteria were diagnosis of WHO I gliomas, ependymomas, metastases, and other nonglial brain tumors and age younger than 12 years.

### MRI Examination

MRI studies were performed with the same 3.0-T MRI unit (Magnetom Verio; Siemens, Erlangen Germany). Diffusion MRI was performed with the following parameters: repetition time, 15 seconds; echo time, 96 msec; eight volumes with  $b = 0$ , 20 volumes with  $b = 700 \text{ sec/mm}^2$ , and 40 volumes with  $b = 2000 \text{ sec/mm}^2$ ; 64 axial sections; field of view,  $256 \times 256 \text{ mm}^2$ ; and isotropic resolution of  $2.0 \times 2.0 \times 2.0 \text{ mm}^3$ . The acquisition time for the diffusion MRI sequence was approximately 20 minutes. The conventional MRI protocol included a T2-weighted turbo spin-echo sequence (repetition time msec/echo time msec, 5420/106; 40 sections; field of view,  $240 \times 240 \text{ mm}^2$ ; voxel size,  $0.47 \times 0.47 \times 3 \text{ mm}^3$ ) and a T1-weighted magnetization-prepared rapid acquisition gradient-echo sequence (repetition time msec/echo time msec/inversion time msec, 1800/2.7/900; nominal isotropic spatial resolution of 1 mm) before and after injection of a gadolinium-based contrast agent (Gadovist, Bayer Schering Pharma, Berlin, Germany; 0.1 mL per kilogram of body weight).

### Image Processing

Diffusion MR images were corrected for motion and eddy current distortions by using ExploreDTI (20), which also corrects the  $b$  matrix accordingly (21). The diffusion tensor was estimated from each shell separately ( $b = 700$  and  $2000 \text{ sec/mm}^2$ ) as well as from both shells combined by using the nonlinear robust estimation of tensors by outlier rejection algorithm in ExploreDTI (22). With the same software, the diffusion kurtosis tensor was estimated from both shells by using the robust extraction of kurtosis indexes with the linear estimation approach (23); mean kurtosis and KA maps were derived. The NODDI model was fitted to both

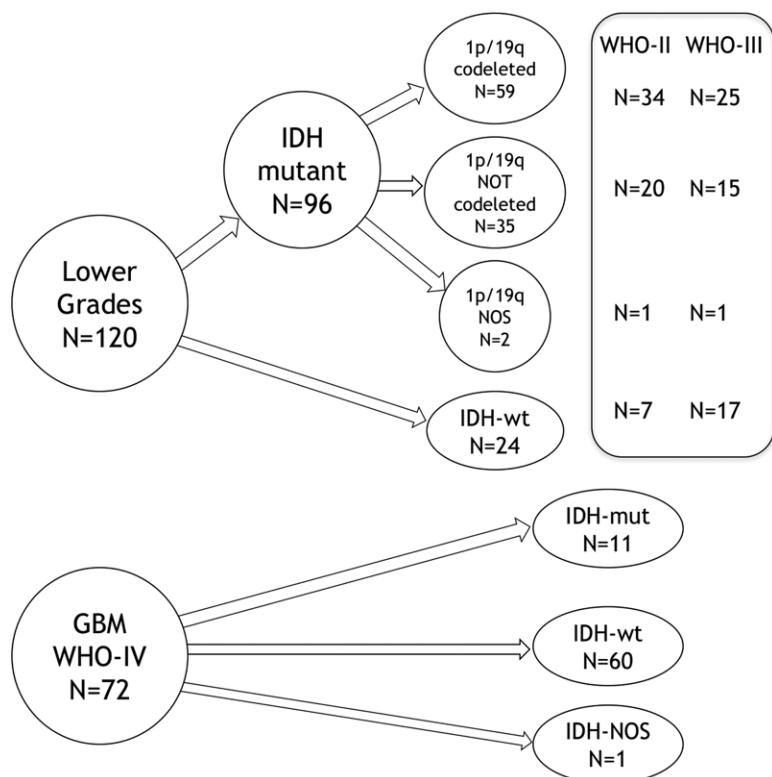


**Figure 1:** Distribution of participants with glioma according to World Health Organization (WHO) grade, isocitrate dehydrogenase (IDH) status, and 1p/19q codeletion. In right column, histopathologic grade is specified for each subgroup of lower-grade glioma. GBM = glioblastoma, mut = mutant, NOS = not otherwise specified, wt = wild type.

shells by using the NODDI Matlab Toolbox (MathWorks, Natick, Mass) (24); restricted fraction (volumetric fraction of the compartment with restricted diffusion in the NODDI model), orientation dispersion index, and isotropic fraction were estimated.

### Diffusion MRI Analysis

Multiple regions of interest (ROIs) were delineated on trace-weighted images obtained with a  $b$  value of 2000 sec/mm<sup>2</sup> in all participants by consensus between a neuroradiologist (A.B., with 20 years of experience in neuroradiology) and a biomedical engineer (M.F., with 5 years of experience in experimental neuro-oncology). ROIs were chosen with the aim of sampling the heterogeneity of the lesion after inspecting T2-weighted images, diffusion-weighted images, MD maps, and postcontrast T1-weighted images. Only the solid parts of each tumor were considered; necrotic areas, cystic intratumoral areas, and areas of presumed perilesional vasogenic edema were excluded from the analysis. On average, three ROIs per participant were delineated. The diameter of the ROI was approximately 8 mm. In each ROI, the mean and standard deviation of the estimated diffusion parameters were computed.

The relationship between the information derived from MRI and that from neuropathologic and genetic analyses was assessed by comparing the values of each diffusion parameter

between the groups defined according to histopathologic characteristics and genetics. Because the latter are provided for a single sample per participant, one ROI mean value per diffusion parameter had to be chosen in each participant. To reflect what is routinely done in neuropathologic examination, where the most aggressive component of the tumor is taken into consideration, and on the basis of the biologic interpretation of diffusion MRI parameters, we selected the maximum values for restricted fraction, isotropic fraction, orientation dispersion index, FA, mean kurtosis, and KA and the minimum value for MD. The same approach was followed in previous DTI studies on this topic (14,15).

### Neuropathologic Examination

Surgery was performed by a team of three board-certified neurosurgeons as previously described (25). Diffusion MR images were available on a neuronavigation system (Brainlab, Munich, Germany). Hyperintense foci at diffusion-weighted imaging were sampled in all patients. One board-certified neuropathologist made all histomolecular diagnoses (B.F., with 12 years of experience). Tumor grade was determined according to the 2007 WHO classification (26). An IDH-1 mutational analysis was conducted with immunohistochemistry analysis by using antibody to IDH R132H in all cases. Wild-type cases were then validated by means of pyrosequencing. The 1p/19q codeletion status was assessed with fluorescence in situ hybridization, and the cell proliferation index was measured with immunohistochemistry analysis by using the MIB-1 antibody against the Ki-67 protein.

### Statistical Analysis

The  $\chi^2$  test was used to compare the hyperintensity on diffusion MR images obtained with a  $b$  value of 2000 sec/mm<sup>2</sup> and contrast enhancement frequencies across groups.

To address the main objective of our study, we first focused on the relationship between diffusion MRI results and groups defined according to IDH mutation genotype. Subsequently, the IDH mutation group was further divided according to 1p/19q phenotype; these two groups were compared among themselves and with IDH wild-type gliomas. Finally, we compared the diffusion metrics among the groups defined according to tumor grade and histotype to be able to relate our results to those of most previous studies.

The Mann-Whitney test was used to evaluate the statistical significance of the differences.  $P < .05$  after Bonferroni correction was considered indicative of a statistically significant difference; all tests for each metric were considered as independent (11 metrics  $\times$  6 tests = 66 comparisons). A receiver operating characteristic curve analysis was also performed for all comparisons.

The McNemar test was used to compare the accuracy between multishell and single-shell models in predicting the IDH

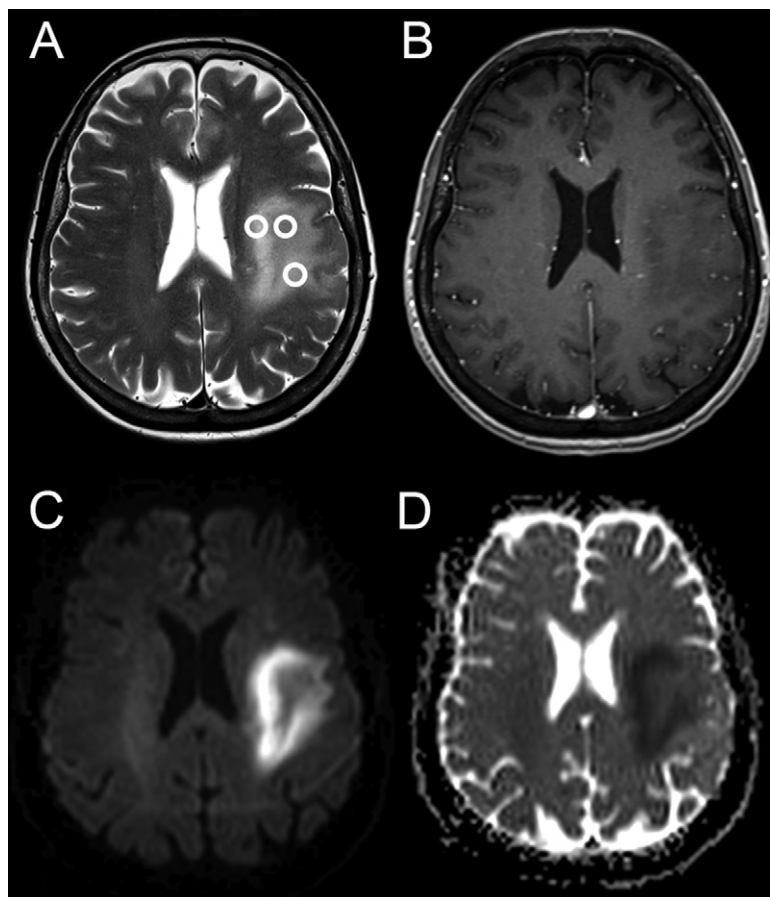


**Figure 2:** Images in 64-year-old woman with astrocytoma isocitrate dehydrogenase wild-type grade II (MIB-1 = 3%) infiltrating dorsal aspect of left arcuate fasciculus in frontoparietal white matter. Axial, *A*, unenhanced T2-weighted MR image, *B*, gadolinium-based contrast agent-enhanced T1-weighted image, *C*, diffusion MR image, and, *D*, mean diffusivity map. Mass is hyperintense on T2-weighted image, with no enhancement after intravenous injection of contrast agent. On diffusion MR image, outer component of mass had high signal intensity, with very low diffusivity. Despite diagnosis of grade II glioma, the patient's overall survival time after surgery was 10 months. To sample tumor diffusivity heterogeneity, round 8-mm-diameter regions of interest were delineated in areas with high, intermediate, and low signal intensity on diffusion MR image. Positions of the three regions of interest used in this participant are indicated in *A*.

wild-type genotype. The absolute difference of the model's accuracy, including the 95% confidence interval, was also computed for each comparison.

The correlation between the MIB-1 proliferation index and each diffusion metric was evaluated with the Pearson correlation coefficient.

## Results

### Participants

Presurgical MRI was performed in 192 participants (113 men, 79 women; mean age, 46.18 years; age range, 14–77 years) with 62 WHO grade II gliomas (35 astrocytomas, 14 oligodendrogliomas, 13 oligoastrocytomas), 58 grade III gliomas (22 astrocytomas, 16 oligodendrogliomas, 20 oligoastrocytomas), and 72 grade IV gliomas (glioblastomas). IDH

genotype was mutant in 55 of the 62 grade II gliomas, 41 of the 58 grade III gliomas, and 11 of the 72 grade IV gliomas. A chart showing stratification according to IDH and 1p/19q status is shown in Figure 1.

### Qualitative Assessment of MR Images

MR images in two representative participants with WHO grade II and grade III IDH wild-type gliomas are shown in Figures 2 and 3, respectively. Hyperintensity on diffusion-weighted images and low MD were present in nine of the 62 grade II gliomas, 31 of the 58 grade III gliomas, and 61 of the 72 grade IV gliomas. Enhancement on postcontrast T1-weighted images was found in five of the 62 grade II gliomas, 24 of the 58 grade III gliomas, and 70 of the 72 grade IV gliomas. Hyperintensity on diffusion-weighted images associated with enhancement occurred in two of the 62 grade II gliomas, 18 of the 58 grade III gliomas, and 60 of the 72 grade IV gliomas. The frequency of hyperintensity and enhancement increased with grade ( $P < .001$ ); however, diffusion hyperintensity tended to be more frequent than enhancement in lower-grade gliomas (although not significantly according to the  $\chi^2$  test,  $P = .26$  for grade II and  $P = .19$  for grade III).

### Correlation of Diffusion MRI Metrics with IDH Genotype and 1p/19q Loss

To test our hypothesis that the occurrence of foci with hyperintensity at diffusion MRI is associated with molecular and histopathologic markers of poor prognosis, we focused on 120 lower-grade gliomas. IDH wild-type gliomas showed significantly higher maximum restricted fraction, maximum KA, and maximum FA, as well as lower minimum MD (derived from the single-shell model with  $b = 2000 \text{ sec/mm}^2$ ), when compared with IDH-mutant gliomas (Fig 4 and Tables 1, 2; unadjusted  $P$  values are in Table E1 [online]). All three models provided at least one significantly different parameter with an effect size larger than 1. Receiver operating characteristic curves are shown in Figure 5, and the associated area under the curve, accuracy, sensitivity, specificity, and positive and negative predictive values are reported in Table 3. The four significantly different metrics had similar areas under the curve, ranging from 0.72 to 0.76. The accuracies of the single-shell versus the multishell model in identifying the correct IDH genotype were not significantly different ( $P > .05$ ), except for minimum MD, which had significantly lower accuracy with respect to maximum restricted fraction ( $P < .001$ ), as reported in Table 4.

In IDH-mutant gliomas, we found no significant difference between participants with and those without 1p/19q codeletion ( $P > .99$  for all after Bonferroni correction)

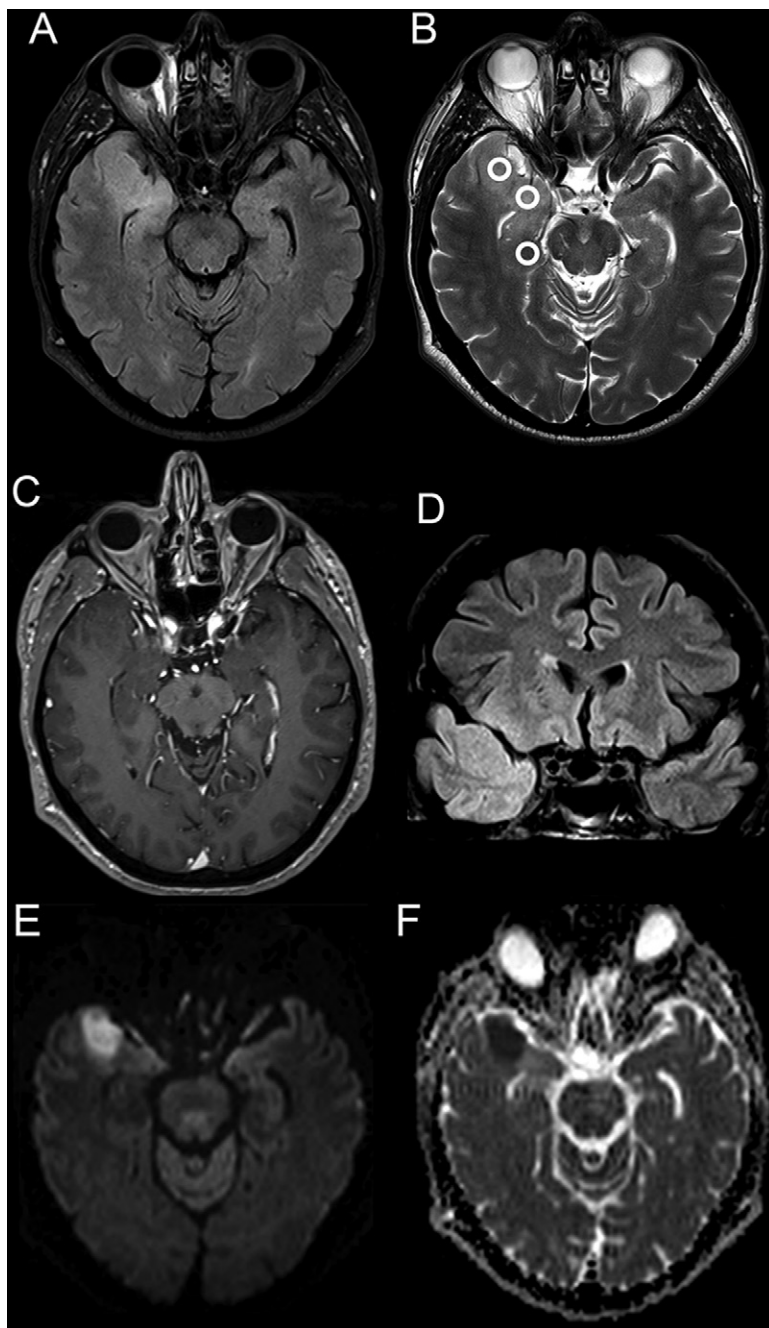


**Figure 3:** Images in 58-year-old man with anaplastic astrocytoma grade III (isocitrate dehydrogenase wild type, MIB-1 = 30%) infiltrating right temporal pole, amygdala, hippocampus, and insula. A, Axial fluid-attenuated inversion-recovery, or FLAIR, B, axial T2-weighted, and, C, axial T1-weighted MR images obtained after injection of gadolinium-based contrast agent and, D, coronal fluid-attenuated inversion-recovery MR image, E, axial diffusion MR image, and, F, mean diffusivity map. Mass is homogeneously hyperintense on T2-weighted fluid-attenuated inversion-recovery image, with no enhancement after intravenous injection of contrast agent. However, the mass has heterogeneous signal intensity on diffusion MR image: The component in the superior aspect of the temporal pole had high signal intensity with very low diffusivity. The component in right hippocampus is hypointense with higher diffusivity. Progression-free survival time was 18 months, followed by a second surgery; overall survival time was 37 months. To sample tumor diffusivity heterogeneity, round 8-mm-diameter regions of interest were delineated in areas with high, intermediate, and low signal intensity on diffusion MR image. Positions of the three regions of interest used in this participant are indicated in B.

(Tables 1, 2). In IDH wild-type gliomas, no significant differences among grades II, III, and IV gliomas were found ( $P > .99$  for all after Bonferroni correction). If we consider grade IV gliomas alone, only maximum KA was significantly different between IDH wild-type and IDH-mutant gliomas ( $P = .039$ ).

### Correlation of Diffusion MRI Metrics with Glioma Grade, Histotype, and Cell Proliferation Index

DTI, diffusion kurtosis imaging, and NODDI metrics of grade IV gliomas were significantly different from those of grade II and III gliomas (Tables 1, 2). Among lower-grade gliomas, none of the metrics were significantly different between grade II and III gliomas or between astrocytomas and oligodendrogliomas (histotype) ( $P > .99$  for all after Bonferroni correction). No correlation was found between any diffusion metric and the cell proliferation index; on the other hand, MIB-1 significantly increased with tumor grade as expected ( $P < .001$  for all comparisons between WHO grades).

### Discussion

Our results showed that minimum MD values were significantly lower and maximum restricted fraction values were significantly higher in IDH wild-type gliomas than in IDH-mutant WHO grade II and III gliomas. Maximum KA and maximum FA values were also significantly higher in IDH wild-type gliomas. These results held true with Bonferroni correction, the most conservative approach to multiple comparison correction (27). The results also showed that the benefit of upgrading the imaging protocol for advanced diffusion models is small, meaning that identification of IDH status with DTI is as good as that with multishell methods.

Recent advances in neuro-oncology have shifted the focus from histopathologic grading to molecular features that have been integrated into the WHO classification. Grading is no longer the most relevant information requested to neuroradiologists, especially in nonenhancing lower-grade gliomas. To stay relevant, imaging must adapt to this paradigm shift and its role should be redirected to identify molecular status. Noninvasive prediction of IDH wild-type lower-grade gliomas is clinically important and challenging. These tumors have a malignant clinical course despite a more indolent appearance on conventional MR images. They also have a lower-grade appearance at histopathologic examination: low cellularity, a low

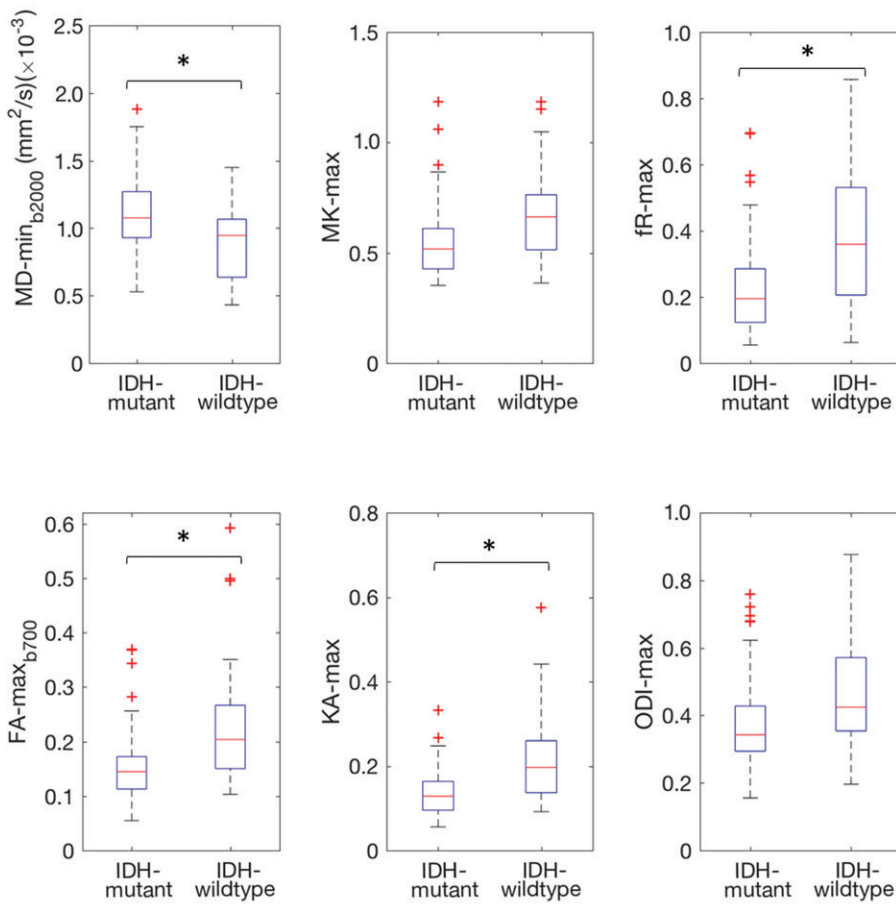


**Figure 4:** Box plots of diffusion-tensor imaging (left), diffusion-kurtosis imaging (middle), and neurite orientation dispersion and density imaging (NODDI) (right) metrics in lower-grade gliomas stratified according to isocitrate dehydrogenase (IDH) status (IDH mutant and IDH wild type). Horizontal red line indicates median, and bottom and top edges of box indicate 25th and 75th percentiles, respectively. Whiskers extend to the most extreme data points not considered outliers. Outliers are plotted individually by using red crosses. FA = fractional anisotropy, fR-max = maximum restricted fraction (volumetric fraction of compartment with restricted diffusion in NODDI model), KA-max = maximum kurtosis anisotropy, MD-min = minimum mean diffusivity, MK-max = maximum mean kurtosis, ODI-max = maximum orientation dispersion index. \* = statistically significant difference ( $P < .05$ ).

mitotic index, and no neoangiogenesis. Thus, DTI might help identify those patients who may benefit from early and more aggressive therapy. It is unlikely that diffusion MRI will replace biopsy to determine tumor genotype; however, it could be used as a surrogate biomarker during follow-up. Currently, only proton MR spectroscopy has been shown to help differentiate IDH mutation in selected patients with glioma. It demonstrates a small signal of 2-hydroxyglutamate in IDH-mutant gliomas. Early studies have shown that MR spectroscopy has a high diagnostic accuracy, but it may be user-dependent (28,29). Its implementation is feasible in highly specialized clinical centers, but it is less accessible than DTI and it may not sample the whole tumor (30).

Using a prospective study design, we confirmed the recently published results by Xiong and colleagues (13–15). The sample size and the effect size in our study are large. Replication of research is very important because it improves precision of prior

knowledge. A key novelty of our study is that we acquired advanced multi-shell diffusion data, which allowed us to further investigate whether more complex models offered any clinical benefit. The benefit gained with advanced models was small in our study. Our comparison of the three models demonstrated that maximum FA was comparable to maximum KA and maximum restricted fraction in the stratification of tumors according to IDH status. This has an impact on clinical applications because DTI metrics can be acquired in less time than multishell data.

An advantage of biophysical models is that they enable biologic interpretation of diffusion data. Traditionally, decreased MD in gliomas has been interpreted as an increase in tumor cellularity (6,12,31–33). This may be true in glioblastomas, which contain foci of very high cellularity. However, we also observed decreased MD in IDH wild-type lower-grade gliomas, where high cellularity is not a reported histopathologic feature. This suggests that the underlying mechanism may be different. A recent PET study with the amino acid *O*-(2-<sup>18</sup>F-fluorethyl)-L-tyrosine showed that radiotracer uptake (ie, high metabolic activity and cellular density) did not co-localize with foci of low diffusivity in nonenhancing lower-grade gliomas, which suggests that tumor cellularity determines a smaller portion of the diffusion MRI signal than other microstructural elements, such as the volume of extracellular space, the distribution of macromolecules in the extracellular matrix, and vessels (34).

We observed increased restricted fraction in the NODDI model, which can be driven either by increased volume of the intracellular space (eg, increased cellularity) or by decreased volume of the extracellular space. Our observations indicate that changes in the volume of the extracellular space may play a role in the modulation of the diffusion signal and may drive the observed changes in restricted fraction, mean kurtosis, and MD. It has been suggested that diffusivity in gliomas may be affected at least in part by decreased hydrophilic components or the expression of hyaluronan in the extracellular matrix (35).

NODDI also helped explain the DTI and diffusion kurtosis imaging anisotropy results: FA and KA were higher in IDH wild-type gliomas than in IDH-mutant lower-grade tumors, which suggests that the integrity of fibers was preserved. On the contrary, the higher orientation dispersion index values suggest

**Table 1: Bonferroni-corrected P Values for All Comparisons and All Considered Diffusion MRI Parameters**

Parameter	IDH-Mutant ( <i>n</i> = 96) vs IDH WT ( <i>n</i> = 24) Glioma (WHO II and III)	IDH-Mutant 1p/19q Codeleted ( <i>n</i> = 59) vs IDH- Mutant 1p/19q Uncodeleted ( <i>n</i> = 60) Glioma (WHO II and III)	IDH-Mutant ( <i>n</i> = 11) vs IDH WT ( <i>n</i> = 60) Glioma (WHO IV)	WHO II vs WHO III	WHO II vs WHO IV	WHO III vs WHO IV
fR-max	.044*	.99	.99	.99	<.001*	<.001*
KA-max	<.001*	.99	.039*	.99	.007*	<.001*
FA-max (both shells)	.065	.99	.99	.99	.133	.018*
FA-max ( <i>b</i> = 700 sec/mm <sup>2</sup> )	.011*	.99	.99	.99	.008*	.003*
FA-max ( <i>b</i> = 2000 sec/mm <sup>2</sup> )	.081	.99	.99	.99	.303	.011*
MD-min (both shells)	.036*	.99	.99	.99	<.001*	<.001*
MD-min ( <i>b</i> = 700 sec/mm <sup>2</sup> )	.069	.99	.99	.99	<.001*	<.001*
MD-min ( <i>b</i> = 2000 sec/mm <sup>2</sup> )	.027*	.99	.99	.99	<.001*	<.001*
MK-max	.122	.99	.99	.99	<.001*	.001*
ODI-max	.353	.99	.99	.666	<.001*	.469
fiso-max	.99	.99	.99	.99	.99	.99

Note.—FA-max = maximum fractional anisotropy, fiso-max = maximum isotropic fraction, fR-max = maximum restricted fraction, IDH = isocitrate dehydrogenase, KA-max = maximum kurtosis anisotropy, MD-min = minimum mean diffusivity, MK-max = maximum mean kurtosis, ODI-max = maximum orientation dispersion index, WHO = World Health Organization, WT = wild type.

\* Significant difference.

**Table 2: Effect Size for All Comparisons and All Considered Diffusion MRI Parameters**

Parameter	IDH-Mutant ( <i>n</i> = 96) vs IDH-WT ( <i>n</i> = 24) Glioma (WHO II and III)	IDH-Mutant 1p/19q Codeleted ( <i>n</i> = 59) vs IDH-Mutant 1p/19q Uncodeleted ( <i>n</i> = 35) Glioma (WHO II and III)	IDH-Mutant ( <i>n</i> = 11) vs IDH-WT ( <i>n</i> = 60) Glioma (WHO IV)	WHO II ( <i>n</i> = 62) vs WHO III ( <i>n</i> = 58)	WHO II ( <i>n</i> = 62) vs WHO IV ( <i>n</i> = 72)	WHO III ( <i>n</i> = 58) vs WHO IV ( <i>n</i> = 72)
fR-max	1.07*	−0.35	0.65 <sup>†</sup>	0.36	1.20*	0.78 <sup>†</sup>
KA-max	1.23*	−0.52	0.90 <sup>†</sup>	0.00	0.72 <sup>†</sup>	0.64 <sup>†</sup>
FA-max (both shells)	1.00*	−0.39	0.64 <sup>†</sup>	−0.10	0.49	0.57 <sup>†</sup>
FA-max ( <i>b</i> = 700 sec/mm <sup>2</sup> )	1.14*	−0.39	0.67 <sup>†</sup>	−0.02	0.64 <sup>†</sup>	0.62 <sup>†</sup>
FA-max ( <i>b</i> = 2000 sec/mm <sup>2</sup> )	0.99 <sup>†</sup>	−0.40	0.64 <sup>†</sup>	−0.14	0.45	0.57 <sup>†</sup>
MD-min (both shells)	−0.88 <sup>†</sup>	0.45	−0.55 <sup>†</sup>	−0.29	−1.29*	−0.90 <sup>†</sup>
MD-min ( <i>b</i> = 700 sec/mm <sup>2</sup> )	−0.88 <sup>†</sup>	0.47	−0.62 <sup>†</sup>	−0.23	−1.18*	−0.89 <sup>†</sup>
MD-min ( <i>b</i> = 2000 sec/mm <sup>2</sup> )	−0.91 <sup>†</sup>	0.45	−0.32	−0.32	−1.36*	−0.93 <sup>†</sup>
MK-max	0.84 <sup>†</sup>	−0.14	0.20	0.34	1.14*	0.78 <sup>†</sup>
ODI-max	0.69 <sup>†</sup>	−0.02	0.10	0.53	1.06*	0.40
fiso-max	−0.49 <sup>†</sup>	0.25	−0.38	0.17	−0.28	−0.50 <sup>†</sup>

Note.—FA-max = maximum fractional anisotropy, fiso-max = maximum isotropic fraction, fR-max = maximum restricted fraction, IDH = isocitrate dehydrogenase, KA-max = maximum kurtosis anisotropy, MD-min = minimum mean diffusivity, MK-max = maximum mean kurtosis, ODI-max = maximum orientation dispersion index, WHO = World Health Organization, WT = wild type.

\* Effect size greater than 1 in absolute value.

<sup>†</sup> Effect size greater than 0.5 in absolute value.

that fibers are actually more dispersed in IDH wild-type gliomas and that, in IDH-mutant gliomas, the higher extracellular water content may be responsible for the decrease in FA and KA. The orientation dispersion index is indeed less affected by excess water content.

We observed no significant differences in diffusion MRI metrics between IDH-mutant gliomas with and without 1p/19q loss. This result also confirmed previous findings by Xiong et al (15). It may indicate either that epigenetic phenotypes do not induce microstructural changes or that diffusion is not sensitive enough to detect these. No significant correlation was found between diffusion MRI metrics and the cell proliferation index. This finding is additional indirect evidence that tumor cellularity may not be the major factor driving increased restricted fraction in lower-grade gliomas. Our findings do not support the results reported by Xiong et al (14), who found significantly lower Ki-67 levels in mutant rather than IDH wild-type oligodendrogliomas.

In the near future, machine learning classifiers using multidimensional datasets may show advantages to univariate methods used in this study. The authors of a recent study with machine learning analysis (36) showed a prediction accuracy of 92% (54 of 59 cases; area under the receiver operating characteristic curve = 0.921), relying on tumor volume and texture information from DTI data of 59 patients with grade II and III glioma.

Limitations of our study must be acknowledged. The ROI-based approach, which was based on tumor characterization with conventional and diffusion MRI, could have introduced operator-dependent variability; however, it allows more flexibility than automated methods. NODDI uses a multicompartement model that has been optimized for normal white matter. In future studies, assumptions must be optimized for pathologic tissues with glioma cells infiltrating and modulating the extracellular matrix.

In conclusion, diffusion metrics from the three models correlated with IDH wild-type in lower-grades gliomas. No significant differences were found among IDH wild-type grade II, III, and IV gliomas. Advanced diffusion MRI models did not add diagnostic accuracy. IDH wild-type lower-grades gliomas tend to be heterogeneous and have foci with reduced diffusivity and higher anisotropy values. These patients may benefit from more aggressive treatments, despite having nonenhancing gliomas on conventional MR images and lacking high-grade features at neuropathologic examination.

**Acknowledgment:** The authors thank Riccardo Pascuzzo, PhD, who provided valuable assistance with the statistical analysis.

**Author contributions:** Guarantor of integrity of entire study, A.B.; study concepts/study design or data acquisition or data analysis/interpretation, all authors; manuscript

drafting or manuscript revision for important intellectual content, all authors; approval of final version of submitted manuscript, all authors; agrees to ensure any questions related to the work are appropriately resolved, all authors; literature research, M.F., M. Grimaldi, G.B., H.Z., A.B.; clinical studies, M.F., M.R., B.F., M. Grimaldi, F.P., L.B., H.Z., A.B.; experimental studies, M. Graham, M. Grimaldi, G.B., F.P., H.Z., A.B.; statistical analysis, M.F., M. Graham, G.M.C., M. Grimaldi, G.B., F.P., H.Z.; and manuscript editing, M.F., M.R., M. Graham, B.F., M. Grimaldi, G.B., F.P., L.B., H.Z., A.B.

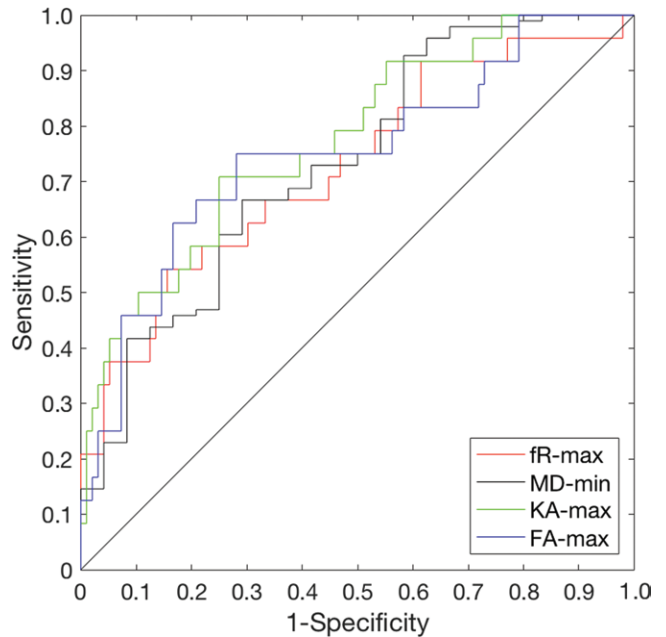


**Figure 5:** Receiver operating characteristic curves for comparison between isocitrate dehydrogenase (IDH) status (IDH mutant or IDH wild type) in lower-grade gliomas. Only those diffusion MRI metrics associated with significant differences between the two groups were reported. Curves show an overall similar performance of the four metrics in differentiating IDH-wildtype and IDH-mutant gliomas. *FA-max* = maximum fractional anisotropy ( $b = 700 \text{ sec/mm}^2$ ), *fR-max* = maximum restricted fraction (volumetric fraction of compartment with restricted diffusion in neurite orientation dispersion and density imaging), *KA-max* = maximum kurtosis anisotropy, *MD-min* = minimum mean diffusivity ( $b = 2000 \text{ sec/mm}^2$ ).

**Table 3: Performance of Diffusion MRI Metrics in the Comparison of IDH-Mutant and IDH Wild-Type Grade II and III Gliomas**

Parameter	MD-min ( $b = 2000 \text{ sec/mm}^2$ )	FA-max ( $b = 700 \text{ sec/mm}^2$ )	KA-max	fR-max
AUC	0.73	0.74	0.76	0.72
Accuracy (%)	68 (81/120)	79 (95/120)	74 (89/120)	78 (94/120)
Sensitivity (%)	71 (17/24)	62 (15/24)	71 (17/24)	54 (13/24)
Specificity (%)	67 (64/96)	83 (80/96)	75 (72/96)	84 (81/96)
PPV (%)	35 (17/49)	48 (15/31)	41 (17/41)	46 (13/28)
NPV (%)	90 (64/71)	90 (80/89)	91 (72/79)	88 (81/92)
Optimal threshold	$9.89 \times 10^{-4} \text{ sec/mm}^2$	0.19	0.16	0.34

Note.—Numbers in parentheses are numbers of participants included for each parameter. Values correspond to the optimal threshold according to the Youden index. AUC = area under the receiver operating characteristic curve, FA-max = maximum fractional anisotropy, fR-max = maximum restricted fraction, IDH = isocitrate dehydrogenase, KA-max = maximum kurtosis anisotropy, MD-min = minimum mean diffusivity, NPV = negative predictive value, PPV = positive predictive value.



**Table 4: Comparison of the Multishell Model against Single-Shell Model in the Prediction of IDH Wild-Type Genotype**

Comparison	Unadjusted <i>P</i> Value*	Difference of Models' Accuracy†
FA-max ( $b = 700 \text{ sec/mm}^2$ ) vs fR-max	.73	0.008 (−0.085, 0.102)
FA-max ( $b = 700 \text{ sec/mm}^2$ ) vs KA-max	.06	0.050 (−0.025, 0.125)
MD-min ( $b = 2000 \text{ sec/mm}^2$ ) vs fR-max	<.001‡	−0.108 (−0.176, −0.040)
MD-min ( $b = 2000 \text{ sec/mm}^2$ ) vs KA-max	.14	−0.067 (−0.142, 0.009)

Note.—Parameters for multishell models were fR-max and KA-max. Parameters for single-shell models were FA-max ( $b = 700 \text{ sec/mm}^2$ ) and MD-min ( $b = 2000 \text{ sec/mm}^2$ ). FA-max = maximum fractional anisotropy, fR-max = maximum restricted fraction, IDH = isocitrate dehydrogenase, KA-max = kurtosis anisotropy, MD-min = mean diffusivity.

\* Determined with the McNemar test.

† Numbers in parentheses are 95% confidence intervals.

‡ Statistically significant ( $P < .0125$ ) with corrected threshold.

**Disclosures of Conflicts of Interest:** M.F. disclosed no relevant relationships. M.R. disclosed no relevant relationships. M.G. disclosed no relevant relationships. G.M.C. disclosed no relevant relationships. B.F. disclosed no relevant relationships. M.G. disclosed no relevant relationships. G.B. disclosed no relevant relationships. E.P. disclosed no relevant relationships. L.B. disclosed no relevant relationships. H.Z. disclosed no relevant relationships. A.B. disclosed no relevant relationships.

## References

- Louis DN, Perry A, Reifenberger G, et al. The 2016 World Health Organization classification of tumors of the central nervous system: a summary. *Acta Neuropathol (Berl)* 2016;131(6):803–820.
- Cancer Genome Atlas Research Network, Brat DJ, Verhaak RG, et al. Comprehensive, integrative genomic analysis of diffuse lower-grade gliomas. *N Engl J Med* 2015;372(26):2481–2498.
- Ohgaki H, Kleihues P. Genetic alterations and signaling pathways in the evolution of gliomas. *Cancer Sci* 2009;100(12):2235–2241.
- Price SJ. Imaging markers of isocitrate dehydrogenase-1 mutations in gliomas. *Neurosurgery* 2015;62(Suppl 1):166–170.
- Basser PJ, Mattiello J, LeBihan D. MR diffusion tensor spectroscopy and imaging. *Biophys J* 1994;66(1):259–267.
- Kono K, Inoue Y, Nakayama K, et al. The role of diffusion-weighted imaging in patients with brain tumors. *AJNR Am J Neuroradiol* 2001;22(6):1081–1088.
- Inoue T, Ogasawara K, Beppu T, Ogawa A, Kabasawa H. Diffusion tensor imaging for preoperative evaluation of tumor grade in gliomas. *Clin Neurol Neurosurg* 2005;107(3):174–180.
- Lee HY, Na DG, Song IC, et al. Diffusion-tensor imaging for glioma grading at 3-T magnetic resonance imaging: analysis of fractional anisotropy and mean diffusivity. *J Comput Assist Tomogr* 2008;32(2):298–303.
- Kang Y, Choi SH, Kim YJ, et al. Gliomas: histogram analysis of apparent diffusion coefficient maps with standard- or high-b-value diffusion-weighted MR imaging—correlation with tumor grade. *Radiology* 2011;261(3):882–890.
- Liu X, Tian W, Kolar B, et al. MR diffusion tensor and perfusion-weighted imaging in preoperative grading of supratentorial nonenhancing gliomas. *Neuro Oncol* 2011;13(4):447–455.
- Server A, Graff BA, Josefsen R, et al. Analysis of diffusion tensor imaging metrics for gliomas grading at 3 T. *Eur J Radiol* 2014;83(3):e156–e165.
- Sugahara T, Korogi Y, Kochi M, et al. Usefulness of diffusion-weighted MRI with echo-planar technique in the evaluation of cellularity in gliomas. *J Magn Reson Imaging* 1999;9(1):53–60.
- Tan WL, Huang WY, Yin B, Xiong J, Wu JS, Geng DY. Can diffusion tensor imaging noninvasively detect IDH1 gene mutations in astroglomas? A retrospective study of 112 cases. *AJNR Am J Neuroradiol* 2014;35(5):920–927.
- Xiong J, Tan WL, Pan JW, et al. Detecting isocitrate dehydrogenase gene mutations in oligodendroglial tumors using diffusion tensor imaging metrics and their correlations with proliferation and microvascular density. *J Magn Reson Imaging* 2016;43(1):45–54.
- Xiong J, Tan W, Wen J, et al. Combination of diffusion tensor imaging and conventional MRI correlates with isocitrate dehydrogenase 1/2 mutations but not 1p/19q genotyping in oligodendroglial tumours. *Eur Radiol* 2016;26(6):1705–1715.
- Jensen JH, Helpert JA, Ramani A, Lu H, Kaczynski K. Diffusional kurtosis imaging: the quantification of non-gaussian water diffusion by means of magnetic resonance imaging. *Magn Reson Med* 2005;53(6):1432–1440.
- Van Cauter S, Veraart J, Sijbers J, et al. Gliomas: diffusion kurtosis MR imaging in grading. *Radiology* 2012;263(2):492–501.
- Bai Y, Lin Y, Tian J, et al. Grading of gliomas by using monoexponential, biexponential, and stretched exponential diffusion-weighted MR imaging and diffusion kurtosis MR imaging. *Radiology* 2016;278(2):496–504.
- Zhang H, Schneider T, Wheeler-Kingshott CA, Alexander DC. NODDI: practical in vivo neurite orientation dispersion and density imaging of the human brain. *Neuroimage* 2012;61(4):1000–1016.
- Leemans A, Jeurissen B, Sijbers J, Jones DK. ExploreDTI: a graphical toolbox for processing, analyzing, and visualizing diffusion MR data [abstr]. In: Proceedings of the Seventeenth Meeting of the International Society for Magnetic Resonance in Medicine. Berkeley, Calif: International Society for Magnetic Resonance in Medicine, 2009; 3537.
- Leemans A, Jones DK. The B-matrix must be rotated when correcting for subject motion in DTI data. *Magn Reson Med* 2009;61(6):1336–1349.
- Chang LC, Jones DK, Pierpaoli C. RESTORE: robust estimation of tensors by outlier rejection. *Magn Reson Med* 2005;53(5):1088–1095.
- Tax CM, Otte WM, Vieregger MA, Dijkhuizen RM, Leemans A. REKINDLE: robust extraction of kurtosis INDICES with linear estimation. *Magn Reson Med* 2015;73(2):794–808.
- Neuroimaging Informatics Tools and Resources Clearinghouse website. [https://www.nitrc.org/projects/noddi\\_toolbox](https://www.nitrc.org/projects/noddi_toolbox). Accessed June 9, 2018.
- Riva M, Fava E, Gallucci M, et al. Monopolar high-frequency language mapping: can it help in the surgical management of gliomas? A comparative clinical study. *J Neurosurg* 2016;124(5):1479–1489.
- Louis DN, Ohgaki H, Wiestler OD, et al. The 2007 WHO classification of tumours of the central nervous system. *Acta Neuropathol* 2007; 14(2):97–109.
- Perneger Tn. What's wrong with Bonferroni adjustments. *BMJ* 1998; 316(7139):1236–1238.
- Choi C, Raisanen JM, Ganji SK, et al. Prospective longitudinal analysis of 2-hydroxyglutarate magnetic resonance spectroscopy identifies broad clinical utility for the management of patients with IDH-mutant glioma. *J Clin Oncol* 2016;34(33):4030–4039.
- Branzoli F, Di Stefano AL, Capelle L, et al. Highly specific determination of IDH status using edited in vivo magnetic resonance spectroscopy. *Neuro Oncol* 2018;20(7):907–916.
- Tietze A, Choi C, Mickey B, et al. Noninvasive assessment of isocitrate dehydrogenase mutation status in cerebral gliomas by magnetic resonance spectroscopy in a clinical setting. *J Neurosurg* 2018;128(2):391–398.
- Chenevert TL, McKeever PE, Ross BD. Monitoring early response of experimental brain tumors to therapy using diffusion magnetic resonance imaging. *Clin Cancer Res* 1997;3(9):1457–1466.
- Gauvain KM, McKinstry RC, Mukherjee P, et al. Evaluating pediatric brain tumor cellularity with diffusion-tensor imaging. *AJR Am J Roentgenol* 2001;177(2):449–454.
- Guo AC, Cummings TJ, Dash RC, Provenzale JM. Lymphomas and high-grade astrocytomas: comparison of water diffusibility and histologic characteristics. *Radiology* 2002;224(1):177–183.
- Rahm V, Boxheimer L, Bruehlmeier M, et al. Focal changes in diffusivity on apparent diffusion coefficient MR imaging and amino acid uptake on PET do not colocalize in nonenhancing low-grade gliomas. *J Nucl Med* 2014;55(4):546–550.
- Sadeghi N, Camby I, Goldman S, et al. Effect of hydrophilic components of the extracellular matrix on quantifiable diffusion-weighted imaging of human gliomas: preliminary results of correlating apparent diffusion coefficient values and hyaluronan expression level. *AJR Am J Roentgenol* 2003;181(1):235–241.
- Eichinger P, Alberts E, Delbridge C, et al. Diffusion tensor image features predict IDH genotype in newly diagnosed WHO grade II/III gliomas. *Sci Rep* 2017;7(1):13396.